

Quantum entanglement swapping between two multipartite entangled states

Xiaolong Su^{1,2,*}, Caixing Tian^{1,2}, Xiaowei Deng^{1,2}, Qiang Li^{1,2}, Changde Xie^{1,2}, and Kunchi Peng^{1,2†}

¹*State Key Laboratory of Quantum Optics and Quantum Optics Devices,
Institute of Opto-Electronics, Shanxi University, Taiyuan, 030006, People's Republic of China*

²*Collaborative Innovation Center of Extreme Optics, Shanxi University,
Taiyuan, Shanxi 030006, People's Republic of China*

Quantum entanglement swapping is one of the most promising ways to realize the quantum connection among local quantum nodes. In this Letter, we present an experimental demonstration of the entanglement swapping between two independent multipartite entangled states, each of which involves a tripartite Greenberger-Horne-Zeilinger (GHZ) entangled state of an optical field. The entanglement swapping is implemented deterministically by means of a joint measurement on two optical modes coming from the two multipartite entangled states respectively and the classical feed-forward of the measurement results. After entanglement swapping the two independent multipartite entangled states are merged into a large entangled state in which all unmeasured quantum modes are entangled. The entanglement swapping between a tripartite GHZ state and an Einstein-Podolsky-Rosen entangled state is also demonstrated and the dependence of the resultant entanglement on transmission loss is investigated. The presented experiment provides a feasible technical reference for constructing more complicated quantum networks.

PACS numbers: 03.67.Hk, 03.67.Bg, 42.50.Ex, 42.50.Lc

Multipartite entangled states play essential roles in quantum computation and quantum networks. Cluster states, a type of multipartite entangled states, are basic quantum resources for one-way quantum computation [1, 2]. Based on a prepared large scale cluster state, one-way quantum computation can be implemented by measurement and feedforward of the measured results [3–6]. It has been demonstrated that a local quantum network can be built by distributing a multipartite entangled state among quantum nodes [7–10]. If we have two space-separated local quantum networks built by two independent multipartite entangled states, respectively, how can we establish entanglement between the quantum nodes in the two local quantum networks? It has been proposed that a large scale cluster state can be generated by the fusion of small scale cluster states, which is completed by means of linear optical elements [11]. The shaping of a larger cluster state to a smaller one according to the requirement for one-way quantum computation has been demonstrated [12]. Another feasible method of merging two multipartite entangled states into one larger multipartite entangled state is quantum entanglement swapping [13], which has been proposed to build a global quantum network of clocks that may allow the construction of a real-time single international time scale (world clock) with unprecedented stability and accuracy [14].

Quantum teleportation enables transportation of an unknown quantum state to a remote station by using an entangled state as the quantum resource. Up to now, long distance quantum teleportation of single pho-

tons over 100 km has been experimentally demonstrated [15–17]. Quantum entanglement swapping, which makes two independent quantum entangled states become entangled without direct interaction, is an important technique in building quantum communication networks [18–26]. Quantum entanglement swapping is also known as quantum teleportation of entangled states [24]. It was originally proposed and demonstrated in discrete-variable optical systems [18, 19], and then it was extended to continuous-variable systems [22–26]. Recently, entanglement swapping between discrete and continuous variable systems has been demonstrated [27], which shows the power of hybrid quantum information processing [28]. The entanglement swapping among three two-photon Einstein-Podolsky-Rosen (EPR) entangled states has been used to generate a Greenberger-Horne-Zeilinger (GHZ) state [29]. However, quantum entanglement swapping between two multipartite entangled states, each of which involves more than two subsystems, has not been demonstrated.

In this Letter, we present the first experimental demonstration of deterministic entanglement swapping between two multipartite entangled states of light. Two multipartite entangled states A and B , consisting of m ($m \geq 2$) and n ($n \geq 2$) optical modes, respectively, are merged into a larger multipartite entangled state C as shown in Fig. 1(a). In order to establish entanglement between the two multipartite entangled states, optical mode A_1 is sent to the multipartite entangled state B through a quantum channel. A joint measurement on modes A_1 and B_1 is implemented and then the measured results are fed forward to the remaining optical modes of state B . The feedforward schemes of measurement results in classical channels depend on the types of quantum correlation of the multipartite entangled state, which are more complex than that for the traditional entanglement

*Electronic address: suxl@sxu.edu.cn

†Electronic address: kcpeng@sxu.edu.cn

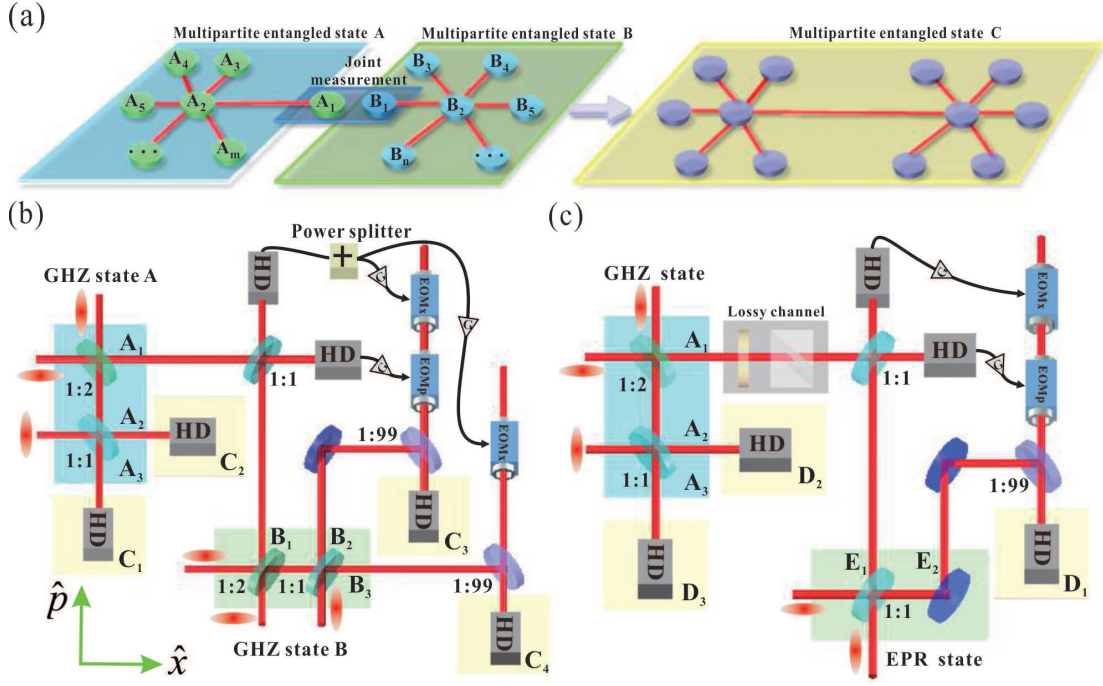


FIG. 1: Schematic of principle and experimental setup. (a) Schematic of entanglement swapping between two multipartite entangled states A and B . The joint measurement is performed on optical modes A_1 and B_1 coming from two multipartite entangled states A and B , respectively. The measurement results are fedforward to the remained quantum modes of multipartite entangled state B . Then a new multipartite entangled state C is obtained after entanglement swapping. (b) The schematic of the experimental setup for the entanglement swapping between two tripartite GHZ entangled states. (c) The schematic of the experimental setup for the entanglement swapping between a tripartite GHZ state and an EPR entangled state. The lossy channel is simulated by a half wave plate and a polarization beam splitter. EOM, electro-optic modulator; HD, homodyne detector. The power splitter is used to split the output photocurrent from the homodyne detector.

swapping between two EPR entangled states. By quantum entanglement swapping, two multipartite entangled states consisting of m and n quantum nodes, respectively, can be merged into a new larger multipartite entangled state consisting of $m + n - 2$ quantum modes, since two modes (A_1 and B_1) have been measured [Fig. 1(a)].

As an example, we experimentally demonstrate the entanglement swapping between two independent tripartite GHZ entangled states consisting of three quantum modes A_1, A_2, A_3 and B_1, B_2, B_3 , respectively [Fig. 1(b)]. Each of the tripartite entangled state of optical field is obtained by combining three squeezed states of light with -5.90 dB squeezing and 9.84 dB anti-squeezing on two optical beam splitters with transmissivity of $1/3$ and $1/2$, respectively [see APPENDIX A]. The amplitude and phase quadratures of an optical mode \hat{a} are expressed by $\hat{x}_a = \hat{a} + \hat{a}^\dagger$ and $\hat{p}_a = (\hat{a} - \hat{a}^\dagger)/i$, respectively. The correlation variances between the amplitude and phase quadratures of three modes A_1 (B_1), A_2 (B_2) and A_3 (B_3) of a tripartite entangled state are expressed by $\Delta^2(\hat{x}_{A_1(B_1)} - \hat{x}_{A_2(B_2)}) = \Delta^2(\hat{x}_{A_2(B_2)} - \hat{x}_{A_3(B_3)}) = \Delta^2(\hat{x}_{A_1(B_1)} - \hat{x}_{A_3(B_3)}) = 2e^{-2r}$ and $\Delta^2(\hat{p}_{A_1(B_1)} + \hat{p}_{A_2(B_2)} + \hat{p}_{A_3(B_3)}) = 3e^{-2r}$, respectively, where the subscripts correspond to different

optical modes and r is the squeezing parameter ($r = 0$ and $r = +\infty$ correspond to no squeezing and the ideally perfect squeezing, respectively). We have suggested that all three squeezed states have identical squeezing and the requirement is easy to be fulfilled in experiments [25].

The \hat{x} -squeezed and \hat{p} -squeezed states are produced by nondegenerate optical parametric amplifiers (NOPAs) pumped by a common laser source, which is a continuous wave intracavity frequency-doubled and frequency-stabilized Nd:YAP/LBO (Nd-doped YAlO_3 perovskite - lithium triborate) laser. The output fundamental wave at 1080 nm wavelength is used for the injected signals of NOPAs and the local oscillators of homodyne detectors. The second-harmonic wave at 540 nm wavelength serves as the pump field of the NOPAs, in which through an intracavity frequency-down-conversion process a pair of signal and idler modes with the identical frequency at 1080 nm and the orthogonal polarizations are generated. Each of the NOPAs consists of an α -cut type-II potassium titanyl phosphate (KTP) crystal and a concave mirror. The front face of the KTP crystal is coated for the input coupler and the concave mirror serves as the output coupler, which is mounted on a piezoelectric transducer to actively lock the cavity length of NOPAs on resonance with the injected signal at 1080 nm. The

transmissivities of the front face of the KTP crystal at 540 nm and 1080 nm are 21.2% and 0.04%, respectively. The end face of the KTP crystal is cut to 1° along the y - z plane of the crystal and is antireflection coated for both 1080 nm and 540 nm [30]. The transmissivities of the output coupler at 540 nm and 1080 nm are 0.5% and 12.5%, respectively. In our experiment, NOPAs are operated at the parametric deamplification situation [30, 31]. Under this condition, the coupled modes at $+45^\circ$ and -45° polarization directions are the \hat{x} -squeezed and \hat{p} -squeezed states, respectively [31].

The joint measurement is performed on modes A_1 and B_1 by a beam splitter and two homodyne detectors. The measurement results are fed forward to the remaining modes in multipartite entangled state B through classical channels, in which $G(\hat{x}_{A_1} - \hat{x}_{B_1})$ and $G(\hat{p}_{A_1} + \hat{p}_{B_1})$ are fed forward to the amplitude and phase quadratures of mode B_2 , and $G(\hat{x}_{A_1} - \hat{x}_{B_1})$ is fed forward to the amplitude quadrature of mode B_3 , respectively, where G is the gain in the classical channels [see APPENDIX B]. The displacement operations are performed by using electro-optical modulators (EOMs) and highly reflecting mirrors (1:99 beam splitters). After entanglement swapping, a new larger multipartite entangled state consisting of four quantum modes (C_1 , C_2 , C_3 , and C_4) is obtained.

The quantum entanglement swapping between a tripartite GHZ state ($m = 3$) and an EPR state ($n = 2$) is also realized, where a new multipartite entangled state D involving three quantum modes (D_1 , D_2 and D_3) is obtained [Fig. 1(c)]. The EPR entangled state is prepared by coupling two squeezed states of light on an optical beam splitter with transmissivity of $1/2$. The joint measurement results on modes A_1 and E_1 , $G(\hat{x}_{A_1} - \hat{x}_{E_1})$ and $G(\hat{p}_{A_1} + \hat{p}_{E_1})$, are fed forward to the amplitude and phase quadratures of mode E_2 through classical channels [see APPENDIX C].

The gain in classical channels is an essential experimental parameter in entanglement swapping [23–25]. The optimal gain $G = 0.95$ for classical channels is applied in the experiment, which reduces the demand for the initial squeezing at the maximal extent. Here, the unit gain is not selected because if $G = 1$ the required squeezing level for obtaining the resultant entangled state is higher than that of $G = 0.95$ [see APPENDIX B and C].

Figure 2 shows the measured quantum correlation variances of the output states. The quantum entanglement among the output modes of multipartite entangled state C is verified by the inseparability criteria for a four-mode GHZ entangled state, which are [32]

$$\begin{aligned} \Delta^2(\hat{x}_{C_1} - \hat{x}_{C_2}) + \Delta^2(\hat{p}_{C_1} + \hat{p}_{C_2} + g_1\hat{p}_{C_3} + g_2\hat{p}_{C_4}) &< 4 \\ \Delta^2(\hat{x}_{C_2} - \hat{x}_{C_3}) + \Delta^2(g_3\hat{p}_{C_1} + \hat{p}_{C_2} + \hat{p}_{C_3} + g_4\hat{p}_{C_4}) &< 4 \\ \Delta^2(\hat{x}_{C_3} - \hat{x}_{C_4}) + \Delta^2(g_5\hat{p}_{C_1} + g_6\hat{p}_{C_2} + \hat{p}_{C_3} + \hat{p}_{C_4}) &< 4 \end{aligned} \quad (1)$$

where g_i ($i = 1, 2, \dots, 6$) is the optimal gain used to minimize the correlation variances at the left-hand sides of Eq. (1). The value 4 at the right-hand sides of Eq. (1) is

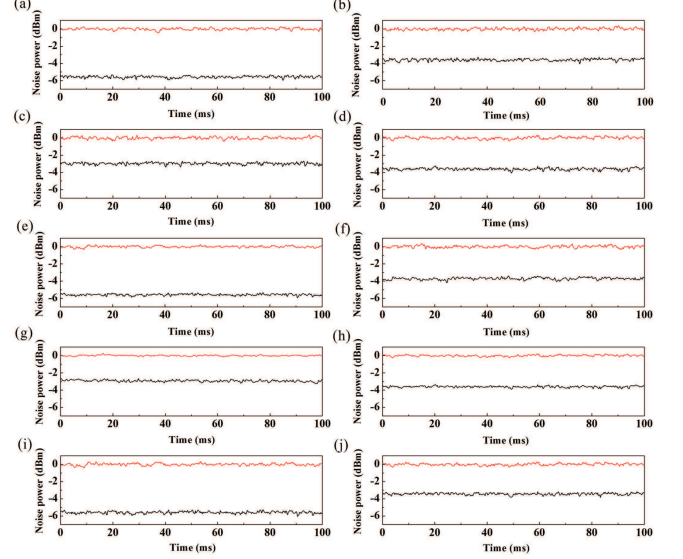


FIG. 2: The measured correlation noises of the output modes. (a)-(f) are the correlation noises for the multipartite entangled state C , which are $\Delta^2(\hat{x}_{C_1} - \hat{x}_{C_2}) = -5.57 \pm 0.12$ dB, $\Delta^2(\hat{p}_{C_1} + \hat{p}_{C_2} + g_1\hat{p}_{C_3} + g_2\hat{p}_{C_4}) = -3.58 \pm 0.13$ dB, $\Delta^2(\hat{x}_{C_2} - \hat{x}_{C_3}) = -2.97 \pm 0.13$ dB, $\Delta^2(g_3\hat{p}_{C_1} + \hat{p}_{C_2} + \hat{p}_{C_3} + g_4\hat{p}_{C_4}) = -3.61 \pm 0.13$ dB, $\Delta^2(\hat{x}_{C_3} - \hat{x}_{C_4}) = -5.59 \pm 0.10$ dB, $\Delta^2(g_5\hat{p}_{C_1} + g_6\hat{p}_{C_2} + \hat{p}_{C_3} + \hat{p}_{C_4}) = -3.71 \pm 0.13$ dB, respectively. (g)-(j) are the correlation noises for the multipartite entangled state D , which are $\Delta^2(\hat{x}_{D_1} - \hat{x}_{D_2}) = -2.93 \pm 0.11$ dB, $\Delta^2(\hat{p}_{D_1} + \hat{p}_{D_2} + g_7\hat{p}_{D_3}) = -3.61 \pm 0.09$ dB, $\Delta^2(\hat{x}_{D_2} - \hat{x}_{D_3}) = -5.59 \pm 0.13$ dB, $\Delta^2(g_8\hat{p}_{D_1} + \hat{p}_{D_2} + \hat{p}_{D_3}) = -3.43 \pm 0.12$ dB, respectively. The red and black lines correspond to the shot noise level and correlation noises, respectively. Measurement frequency is 3 MHz, parameters of the spectrum analyzer: resolution bandwidth is 30 kHz, and video bandwidth is 300 Hz.

the corresponding boundary for inseparability. When all correlation variances at the left-hand sides of Eq. (1) are smaller than 4, four modes C_1 , C_2 , C_3 , and C_4 are entangled. From the measured results shown in Figs. 2(a)-2(f), we can calculate the combinations of correlation variances at the left-hand sides of the three inequalities, which are 2.10 ± 0.06 , 2.65 ± 0.08 , and 2.06 ± 0.06 with $g_1 = 0.90$, $g_2 = 0.84$, $g_3 = g_4 = 0.94$, and $g_5 = g_6 = 0.88$, respectively. The satisfaction of the inseparability criteria of the four-mode GHZ state confirms the success of quantum entanglement swapping between two tripartite GHZ entangled states of light.

The inseparability criteria for a three-mode GHZ entangled state established in the entanglement swapping between the tripartite entangled state and the EPR entangled state are given by

$$\begin{aligned} \Delta^2(\hat{x}_{D_1} - \hat{x}_{D_2}) + \Delta^2(\hat{p}_{D_1} + \hat{p}_{D_2} + g_7\hat{p}_{D_3}) &< 4 \quad (2) \\ \Delta^2(\hat{x}_{D_2} - \hat{x}_{D_3}) + \Delta^2(g_8\hat{p}_{D_1} + \hat{p}_{D_2} + \hat{p}_{D_3}) &< 4 \end{aligned}$$

where g_j ($j = 7, 8$) is the optimal gain used to minimize the correlation variances at the left-hand sides of

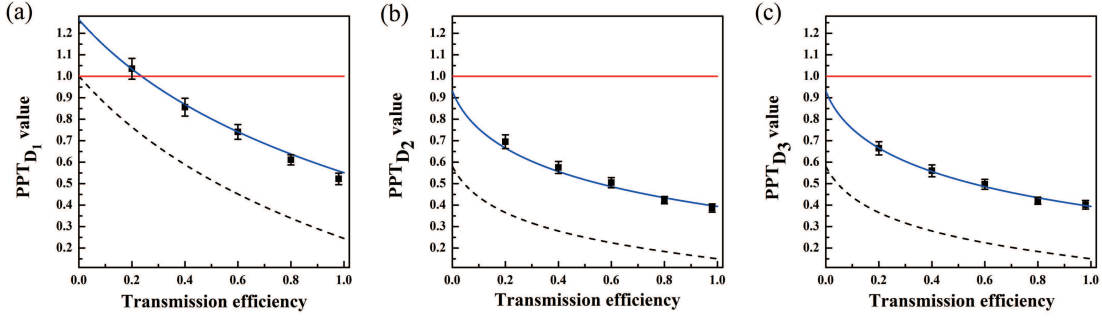


FIG. 3: The distributed entanglement in a lossy channel. (a)-(c), The PPT values PPT_{D_1} , PPT_{D_2} and PPT_{D_3} represent the different splittings for the $(D_1|D_2D_3)$, $(D_2|D_1D_3)$, and $(D_3|D_1D_2)$, respectively, which measure the inseparability of one mode with the other two modes. The PPT values in a lossy channel (blue lines) are all below the boundary (red lines) when channel efficiency is higher than 0.24. The dashed lines are the obtained PPT values with -10.9 dB squeezing, which shows that the obtained tripartite entanglement can be robust against loss in the quantum channel. The black dots represent the experimental data. Error bars represent ± 1 standard deviation and are obtained based on the statistics of the measured noise variances.

Eq. (2). From the measured results shown in Figs. 2(g)-2(j), we obtain the values at the left-hand sides of Eq. (2), which are 2.27 ± 0.06 and 1.85 ± 0.05 with $g_7 = 0.94$, $g_8 = 0.93$, respectively. The values are smaller than 4 and thus demonstrate the success of entanglement swapping between the tripartite entangled state and the EPR entangled state.

We also consider the feasibility of completing entanglement swapping in a real quantum communication network. In quantum communication, the losses and noises in quantum channels lead to decoherence of quantum states and the distributed entanglement will degrade (even disappear) by the unavoidable decoherence. We simulate the loss in real quantum channels by using a half wave plate and a polarization beam splitter as shown in Fig. 1(c). The positive partial transposition (PPT) criterion is a necessary and sufficient condition for judging the existence of quantum entanglement among N Gaussian optical beams, when the state has the form of bipartite splitting with only a single mode on one side like $(1|N-1)$ [33–35]. We characterize the features of quantum entanglement reduction when an optical mode is transmitted over a lossy channel with the PPT criterion.

The PPT values are symplectic eigenvalues of a partially transposed matrix. At the level of quadrature operators, the partial transposition with respect to mode k ($k = 1, 2, 3$) corresponds to the change of sign of phase quadrature, $\hat{p}_k \rightarrow -\hat{p}_k$. Symplectic eigenvalues of covariance matrix are defined as positive roots of polynomial $|\gamma^{T(k)} - i\mu\Omega| = 0$, where $|A|$ denotes the determinant of matrix [35]. $\gamma^{T(k)} = T_k \gamma T_k^T$ is the partially transposed matrix of the quantum state, where T_k is a diagonal matrix with all diagonal elements equal to 1 except for $T_{2k,2k} = -1$, and

$$\Omega = \oplus_{k=1}^3 \begin{pmatrix} 0 & 1 \\ -1 & 0 \end{pmatrix}. \quad (3)$$

We consider a bipartite splitting of a three-mode Gaus-

sian state with covariance matrix γ such that one party holds mode k and the other party possesses the remaining two modes. If the smallest symplectic eigenvalue μ_k obtained from the polynomial is below 1, the state is inseparable with respect to the $k|ij$ splitting.

As shown in Fig. 3, the output optical modes are entangled if the channel efficiency is larger than 0.24 at the present squeezing level, where the optimal gain in classical channel is chosen to be $G = 0.85$ according to the requirement of the PPT criterion. If we consider transmission in a fiber with a loss of 0.2 dB/km, the achievable transmission distance will be about 30 km. Since the optical mode D_1 comes from the network B while D_2 and D_3 come from the network A , the PPT value of $(D_1|D_2D_3)$ is more sensitive to loss than other two PPT values. The output entangled state will be more robust against loss in a quantum channel when the squeezing of resource states increases. For example, when the squeezing is -10.9 dB, which has been realized by H. Vahlbruch *et al.* [36], the obtained entanglement will be quite robust against loss (dashed-line in Fig. 3). The PPT values in Figs. 3(b) and 3(c) are smaller than the boundary even when the transmission efficiency in the quantum channel is zero, and this is because the optical modes D_2 and D_3 come from the same local network and they are entangled initially.

In summary, we experimentally demonstrate quantum entanglement swapping between two multipartite GHZ entangled states. After the quantum entanglement swapping of multipartite entangled states, the quantum modes, more than two in two multipartite entangled states that never interacted directly, become entangled. In the experiment, GHZ entangled states are used as the quantum resources for entanglement swapping. In principle, this method may also be extended to construct large scale cluster states, which are very useful for quantum computation. Of course, because quantum correlation in cluster states is different from that in GHZ states, the

corresponding feedforward scheme needs to be designed according to different requirements.

The entanglement swapping between a tripartite GHZ state and an EPR entangled state through a lossy channel equivalent to an optical fiber of 30 km is achieved at present squeezing level. The robustness of the distributed entanglement over lossy channels depends on the initial squeezing of multipartite entangled states. Squeezing over 15 dB has been experimentally generated [36], the use of which will increase the distance of the entanglement swapping significantly. The robustness of the distributed entanglement over lossy channels can also be improved by using the existent techniques. For example, the noiseless linear amplification [37–39], can be used in the system to improve the quality of entanglement swapping in a lossy channel. When the quantum channel is a noisy channel, the noise of which is higher than the vacuum noise, a correlated noisy channel can be used to remove the effect of noise on entangled states [40]. Since a local quantum network can be established by distributing a multipartite entangled state to different quantum nodes, the presented scheme can be used to merge two space-separated local quantum networks into a large quantum network.

This research was supported by the National Natural Science Foundation of China (NSFC) (Grants No. 11522433, No. 61475092), the program of Youth Sanjin Scholar and National Basic Research Program of China (Grant No. 2016YFA0301402).

APPENDIX

A. Preparation of the tripartite entangled states

As shown in Fig. 1 in the maintext, the tripartite Greenberger-Horne-Zeilinger (GHZ) state A of optical field is prepared by coupling a phase-squeezed state (\hat{a}_2) of light and two amplitude-squeezed states of light (\hat{a}_1 and \hat{a}_3) on an optical beam-splitter network, which consists of two optical beam-splitters with transmittance of $T_{A1} = 1/3$ and $T_{A2} = 1/2$, respectively. The other tripartite GHZ state B of optical field is prepared by coupling a amplitude-squeezed state (\hat{b}_3) of light and two phase-squeezed states of light (\hat{b}_1 and \hat{b}_2) on an optical beam-splitter network, which consists of two optical beam-splitters with transmittance of $T_{B1} = 1/3$ and $T_{B2} = 1/2$, respectively. The transformation matrixes of the beam-splitter networks for establishing tripartite GHZ entangled states A and B are given by

$$U_A = \begin{bmatrix} \sqrt{\frac{2}{3}} & \sqrt{\frac{1}{3}} & 0 \\ -\sqrt{\frac{1}{6}} & \sqrt{\frac{1}{3}} & \sqrt{\frac{1}{2}} \\ -\sqrt{\frac{1}{6}} & \sqrt{\frac{1}{3}} & -\sqrt{\frac{1}{2}} \end{bmatrix}, \quad (4)$$

$$U_B = \begin{bmatrix} i\sqrt{\frac{2}{3}} & \sqrt{\frac{1}{3}} & 0 \\ -i\sqrt{\frac{1}{6}} & \sqrt{\frac{1}{3}} & \sqrt{\frac{1}{2}} \\ -i\sqrt{\frac{1}{6}} & \sqrt{\frac{1}{3}} & -\sqrt{\frac{1}{2}} \end{bmatrix}, \quad (5)$$

respectively. The unitary matrix can be decomposed into a beam-splitter network $U_A = B_{23}^+(T_{A2})I_2(-1)B_{12}^+(T_{A1})$, $U_B = B_{23}^+(T_{B2})I_2(-1)B_{12}^+(T_{B1})F_1$, where $B_{kl}^+(T_j)$ stands for the linearly optical transformation on j -th beam-splitter with transmissivity of $T_{Aj(Bj)}$ ($j = 1, 2$), $(B_{kl}^+)_{kk} = \sqrt{1-T}$, $(B_{kl}^+)_{kl} = (B_{kl}^+)_{lk} = \sqrt{T}$, $(B_{kl}^+)_{ll} = -\sqrt{1-T}$, are matrix elements of the beam-splitter. $I_k(-1) = e^{i\pi}$ corresponds to a 180° rotation in phase space and $F_1 = e^{i\frac{\pi}{2}}$ corresponds to a Fourier transformation in phase space. The output modes from the optical beam-splitter network are expressed by

$$\begin{aligned} A_1 &= \sqrt{\frac{2}{3}}\hat{a}_1 + \sqrt{\frac{1}{3}}\hat{a}_2, \\ A_2 &= -\sqrt{\frac{1}{6}}\hat{a}_1 + \sqrt{\frac{1}{3}}\hat{a}_2 + \sqrt{\frac{1}{2}}\hat{a}_3, \\ A_3 &= -\sqrt{\frac{1}{6}}\hat{a}_1 + \sqrt{\frac{1}{3}}\hat{a}_2 - \sqrt{\frac{1}{2}}\hat{a}_3, \\ B_1 &= i\sqrt{\frac{2}{3}}\hat{b}_1 + \sqrt{\frac{1}{3}}\hat{b}_2, \\ B_2 &= -i\sqrt{\frac{1}{6}}\hat{b}_1 + \sqrt{\frac{1}{3}}\hat{b}_2 + \sqrt{\frac{1}{2}}\hat{b}_3, \\ B_3 &= -i\sqrt{\frac{1}{6}}\hat{b}_1 + \sqrt{\frac{1}{3}}\hat{b}_2 - \sqrt{\frac{1}{2}}\hat{b}_3, \end{aligned} \quad (6)$$

respectively. The quantum correlation noises of two tripartite GHZ states are given by

$$\begin{aligned} \hat{x}_{A1} - \hat{x}_{A2} &= \sqrt{\frac{3}{2}}\hat{x}_{a1}^{(0)}e^{-r} - \sqrt{\frac{1}{2}}\hat{x}_{a3}^{(0)}e^{-r}, \\ \hat{x}_{A2} - \hat{x}_{A3} &= \sqrt{2}\hat{x}_{a3}^{(0)}e^{-r}, \\ \hat{x}_{A1} - \hat{x}_{A3} &= \sqrt{\frac{3}{2}}\hat{x}_{a1}^{(0)}e^{-r} + \sqrt{\frac{1}{2}}\hat{x}_{a3}^{(0)}e^{-r}, \\ \hat{p}_{A1} + \hat{p}_{A2} + \hat{p}_{A3} &= \sqrt{3}\hat{p}_{a2}^{(0)}e^{-r}, \\ \hat{x}_{B1} - \hat{x}_{B2} &= -\sqrt{\frac{3}{2}}\hat{p}_{b1}^{(0)}e^{-r} - \sqrt{\frac{1}{2}}\hat{x}_{b3}^{(0)}e^{-r}, \\ \hat{x}_{B2} - \hat{x}_{B3} &= \sqrt{2}\hat{x}_{b3}^{(0)}e^{-r}, \\ \hat{x}_{B1} - \hat{x}_{B3} &= -\sqrt{\frac{3}{2}}\hat{p}_{b1}^{(0)}e^{-r} + \sqrt{\frac{1}{2}}\hat{x}_{b3}^{(0)}e^{-r}, \\ \hat{p}_{B1} + \hat{p}_{B2} + \hat{p}_{B3} &= \sqrt{3}\hat{p}_{b2}^{(0)}e^{-r}, \end{aligned} \quad (7)$$

respectively, where $\hat{x}_j^{(0)}$ and $\hat{p}_j^{(0)}$ denote the quadrature-amplitude and the quadrature-phase operators of corresponding vacuum field, respectively, and r is the squeezing parameter ($r = 0$ and $r = +\infty$ correspond to no squeezing and the ideally perfect squeezing, respectively).

Here, we have assumed that six squeezed states have the identical squeezing parameter. In the experiment, this requirement is easily achieved by adjusting the three non-degenerate optical parametric amplifiers (NOPAs) to be operated at the same conditions.

Fig. 4 shows the experimentally measured quantum correlation noises for the prepared tripartite GHZ entangled state A. The inseparability criteria for a tripartite GHZ entangled state is given by [32]

$$\begin{aligned} \langle \Delta^2(\hat{x}_{A_1} - \hat{x}_{A_2}) \rangle + \langle \Delta^2(\hat{p}_{A_1} + \hat{p}_{A_2} + \hat{p}_{A_3}) \rangle &< 4, \\ \langle \Delta^2(\hat{x}_{A_2} - \hat{x}_{A_3}) \rangle + \langle \Delta^2(\hat{p}_{A_1} + \hat{p}_{A_2} + \hat{p}_{A_3}) \rangle &< 4. \end{aligned} \quad (8)$$

From the measured quantum correlation noises, the calculated values of the left-hand sides of inequalities (8) are 1.37 ± 0.04 and 1.34 ± 0.04 , respectively, which confirm that the three optical modes are in a tripartite GHZ entangled state.

B. Entanglement swapping between two tripartite GHZ states

The optical mode A_1 is transmitted from multipartite entangled state A to multipartite entangled state B and mixed with B_1 on a 1:1 beam-splitter. The output modes μ and ν are measured by two homodyne detectors yield classical photocurrents for the quadratures \hat{x}_ν and \hat{p}_μ , which are

$$\begin{aligned} \hat{p}_\mu &= \frac{1}{\sqrt{2}}(\hat{p}_{A_1} + \hat{p}_{B_1}), \\ \hat{x}_\nu &= \frac{1}{\sqrt{2}}(\hat{x}_{A_1} - \hat{x}_{B_1}), \end{aligned} \quad (9)$$

respectively. The measurement results of $\sqrt{2}G(\hat{x}_\nu + \hat{p}_\mu)$ and $\sqrt{2}G\hat{x}_\nu$ are fed forward to B_2 and B_3 , respectively. The amplitude and phase quadratures of output states are expressed by

$$\begin{aligned} \hat{x}_{C_1} &= \hat{x}_{A_3}, \\ \hat{p}_{C_1} &= \hat{p}_{A_3}, \\ \hat{x}_{C_2} &= \hat{x}_{A_2}, \\ \hat{p}_{C_2} &= \hat{p}_{A_2}, \\ \hat{x}_{C_3} &= \hat{x}_{B_2} + \sqrt{2}G\hat{x}_\nu, \\ \hat{p}_{C_3} &= \hat{p}_{B_2} + \sqrt{2}G\hat{p}_\mu, \\ \hat{x}_{C_4} &= \hat{x}_{B_3} + \sqrt{2}G\hat{x}_\nu, \\ \hat{p}_{C_4} &= \hat{p}_{B_3}, \end{aligned} \quad (10)$$

respectively. The parameter G describes the gain in classical channel.

The quantum entanglement among the output modes in multipartite entangled state C is verified by the inseparability criteria for a four-mode GHZ entangled state

[32], which are

$$\begin{aligned} \Delta^2(\hat{x}_{C_1} - \hat{x}_{C_2}) + \Delta^2(\hat{p}_{C_1} + \hat{p}_{C_2} + g_1\hat{p}_{C_3} + g_2\hat{p}_{C_4}) &< 4, \\ \Delta^2(\hat{x}_{C_2} - \hat{x}_{C_3}) + \Delta^2(g_3\hat{p}_{C_1} + \hat{p}_{C_2} + \hat{p}_{C_3} + g_4\hat{p}_{C_4}) &< 4, \\ \Delta^2(\hat{x}_{C_3} - \hat{x}_{C_4}) + \Delta^2(g_5\hat{p}_{C_1} + g_6\hat{p}_{C_2} + \hat{p}_{C_3} + \hat{p}_{C_4}) &< 4, \end{aligned} \quad (11)$$

where g_i ($i = 1, 2, \dots, 6$) is the optimal gain used to minimize the correlation variances at the left-hand sides of Eq. (11).

The correlation variances of quadrature components among the output states are expressed by

$$\begin{aligned} V_1 &= \langle \Delta^2(\hat{x}_{C_1} - \hat{x}_{C_2}) \rangle = 2V, \\ V_2 &= \langle \Delta^2(\hat{p}_{C_1} + \hat{p}_{C_2} + g_1\hat{p}_{C_3} + g_2\hat{p}_{C_4}) \rangle \\ &= \frac{[(2 + Gg_1)^2 + (g_1 + Gg_1 + g_2)^2]V}{3} \\ &\quad + \frac{[4(Gg_1 - 1)^2 + 3(g_1 - g_2)^2 + (g_1 - 2Gg_1 + g_2)^2]V'}{6}, \\ V_3 &= \langle \Delta^2(\hat{x}_{C_2} - \hat{x}_{C_3}) \rangle \\ &= \frac{2[(G - 1)^2V' + 2(1 + G + G^2)V]}{3}, \\ V_4 &= \langle \Delta^2(g_3\hat{p}_{C_1} + \hat{p}_{C_2} + \hat{p}_{C_3} + g_4\hat{p}_{C_4}) \rangle \\ &= \frac{[(1 + G + g_3)^2 + (1 + g_4 + G)^2]V}{3} \\ &\quad + \frac{[(2G - 1 - g_3)^2 + 3(1 - g_3)^2]V'}{6} \\ &\quad + \frac{(2G - g_4 - 1)^2 + 3(1 - g_4)^2V'}{6}, \\ V_5 &= \langle \Delta^2(\hat{x}_{C_3} - \hat{x}_{C_4}) \rangle = 2V, \\ V_6 &= \langle \Delta^2(g_5\hat{p}_{C_1} + g_6\hat{p}_{C_2} + \hat{p}_{C_3} + \hat{p}_{C_4}) \rangle \\ &= \frac{[(G + g_5 + g_6)^2 + (2 + G)^2]V}{3} \\ &\quad + \frac{[(2G - g_5 - g_6)^2 + 3(g_6 - g_5)^2 + (2G - 2)^2]V'}{6}, \end{aligned} \quad (12)$$

respectively, where $V = e^{-2r}$ and $V' = e^{2r}$ represent the variances of squeezed and anti-squeezed quadratures of the optical mode, respectively. The optimal gain in classical channel equals to

$$G = \frac{V' - V}{V' + V}. \quad (13)$$

The calculated optimal gain g_i ($i = 1, 2, \dots, 6$) are

$$\begin{aligned} g_1 &= \frac{2(V' - V)^2(V' + V)(2V' + V)}{4V'^4 + 14V'^3V + 9V'^2V^2 + 8V'V^3 + V^4}, \\ g_2 &= \frac{4V'(V' - V)^3}{4V'^4 + 14V'^3V + 9V'^2V^2 + 8V'V^3 + V^4}, \end{aligned} \quad (14)$$

(15)

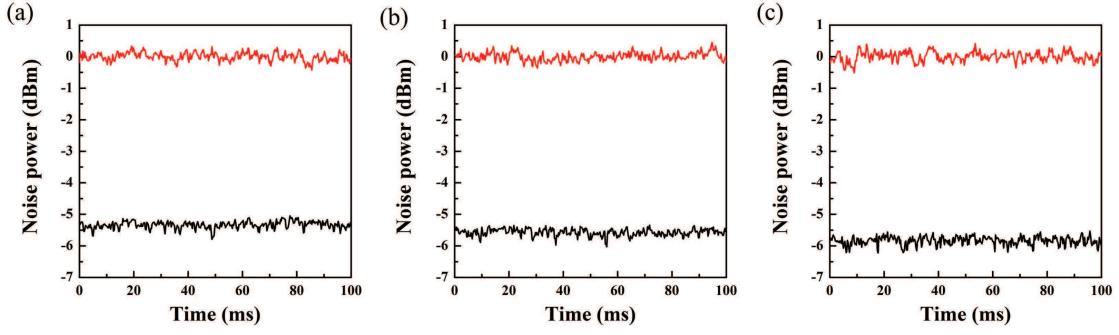


FIG. 4: **The measured quantum correlation noises for the prepared tripartite GHZ entangled state A.** (a) - (c), The measured the correlation noises are $\Delta^2(x_{A_1} - x_{A_2}) = -5.34 \pm 0.11$ dB, $\Delta^2(\hat{x}_{A_2} - \hat{x}_{A_3}) = -5.57 \pm 0.11$ dB, $\Delta^2(\hat{p}_{A_1} + \hat{p}_{A_2} + \hat{p}_{A_3}) = -5.84 \pm 0.13$ dB, respectively. The red and black lines correspond to the shot noise level and correlation noises, respectively. Measurement frequency is 3 MHz, parameters of the spectrum analyzer: resolution bandwidth is 30 kHz, and video bandwidth is 300 Hz.

$$\begin{aligned}
 g_3 &= \frac{2(V'^2 - V'V)}{(V' + V)(2V' + V)}, \\
 g_4 &= \frac{2(V'^2 - V'V)}{(V' + V)(2V' + V)}, \\
 g_5 &= \frac{(V' - V)^2}{(V' + V)(V' + 2V)}, \\
 g_6 &= \frac{(V' - V)^2}{(V' + V)(V' + 2V)}.
 \end{aligned}$$

Fig. 5 shows the dependence of inseparability criteria of four-mode GHZ entangled state on squeezing parameter. The optimal gains g_i ($i = 1, 2, \dots, 6$) in Eq. (14) are chosen in the calculation. If the unit gain is chosen, the obtained state is entangled only when the squeezing parameter is higher than 0.44 (-3.82 dB squeezing, dashed lines). However, when optimal gain factor $G = 0.95$ is used, the requirement of entanglement on the squeezing parameter is reduced (solid lines).

C. Entanglement swapping between a tripartite GHZ state and an EPR state

The EPR entangled state is prepared by coupling a phase-squeezed state (\hat{b}_1) of light and a amplitude-squeezed state of light (\hat{b}_2) on a 1:1 beam-splitter, the output states are

$$\begin{aligned}
 E_1 &= \frac{1}{\sqrt{2}}(\hat{b}_1 + \hat{b}_2), \\
 E_2 &= \frac{1}{\sqrt{2}}(\hat{b}_1 - \hat{b}_2),
 \end{aligned} \tag{16}$$

respectively. The quantum correlations between the amplitude and phase quadratures of the EPR entangled state are $\Delta^2(\hat{x}_{E_1} - \hat{x}_{E_2}) = \Delta^2(\hat{p}_{E_1} + \hat{p}_{E_2}) = 2e^{-2r}$.

After the transmission of optical mode \hat{A}_1 over a lossy channel, the output mode is given by $\hat{A}_L = \sqrt{\eta}\hat{A}_1 +$

$\sqrt{1-\eta}\hat{v}_0$, where η and \hat{v}_0 represent the transmission efficiency of quantum channel and vacuum state induced by loss into the quantum channel, respectively. Then modes A_L and E_1 are combined by a 1:1 beam splitter, the output modes of the beam-splitter are measured by two homodyne detectors yield classical photocurrents for the quadratures \hat{x}_v and \hat{p}_μ , which are

$$\begin{aligned}
 \hat{p}_\mu &= \frac{1}{\sqrt{2}}(\hat{p}_{A_L} + \hat{p}_{E_1}), \\
 \hat{x}_v &= \frac{1}{\sqrt{2}}(\hat{x}_{A_L} - \hat{x}_{E_1}),
 \end{aligned} \tag{17}$$

respectively. The measurement results of $\sqrt{2}G\hat{x}_v$ and $\sqrt{2}G\hat{p}_\mu$ are fed forward to E_2 . The quadratures of output states are expressed by

$$\begin{aligned}
 \hat{x}_{D_1} &= \hat{x}_{E_2} + \sqrt{2}G\hat{x}_v, \\
 \hat{p}_{D_1} &= \hat{p}_{E_2} + \sqrt{2}G\hat{p}_\mu, \\
 \hat{x}_{D_2} &= \hat{x}_{A_2}, \\
 \hat{p}_{D_2} &= \hat{p}_{A_2}, \\
 \hat{x}_{D_3} &= \hat{x}_{A_3}, \\
 \hat{p}_{D_3} &= \hat{p}_{A_3},
 \end{aligned} \tag{18}$$

respectively.

The inseparability criteria for a three-mode GHZ entangled state established in the entanglement swapping between a tripartite GHZ state and an EPR entangled state are given by [32]

$$\begin{aligned}
 \Delta^2(\hat{x}_{D_1} - \hat{x}_{D_2}) + \Delta^2(\hat{p}_{D_1} + \hat{p}_{D_2} + g_7\hat{p}_{D_3}) &< 4, \\
 \Delta^2(\hat{x}_{D_2} - \hat{x}_{D_3}) + \Delta^2(g_8\hat{p}_{D_1} + \hat{p}_{D_2} + \hat{p}_{D_3}) &< 4,
 \end{aligned} \tag{19}$$

where g_j ($j = 7, 8$) is the optimal gain used to minimize the correlation variances at the left-hand sides of Eq. (19). When $\eta = 1$, the correlation variances of quadrature components among the output states are expressed

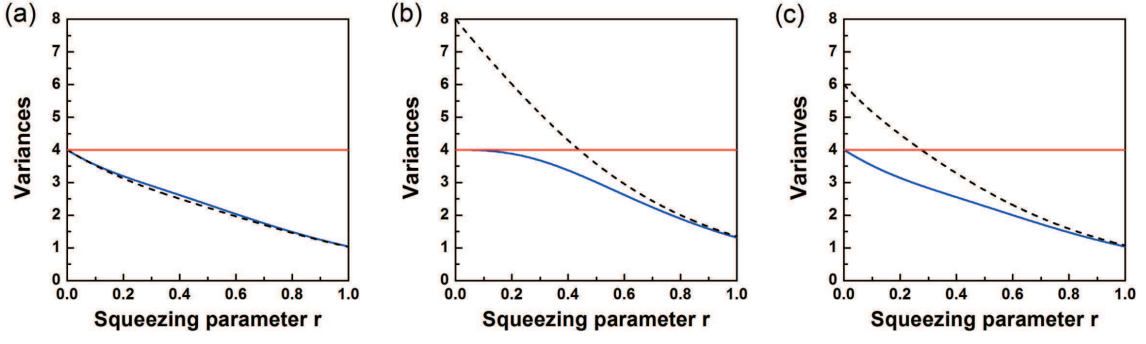


FIG. 5: **The inseparability criteria for the obtained four-mode GHZ entangled state.** (a) - (c) are corresponding to the first, second and third inequalities in Eq. (11), respectively. The dashed and solid lines correspond to the case of unit and optimal gain factor in the classical channel, respectively.

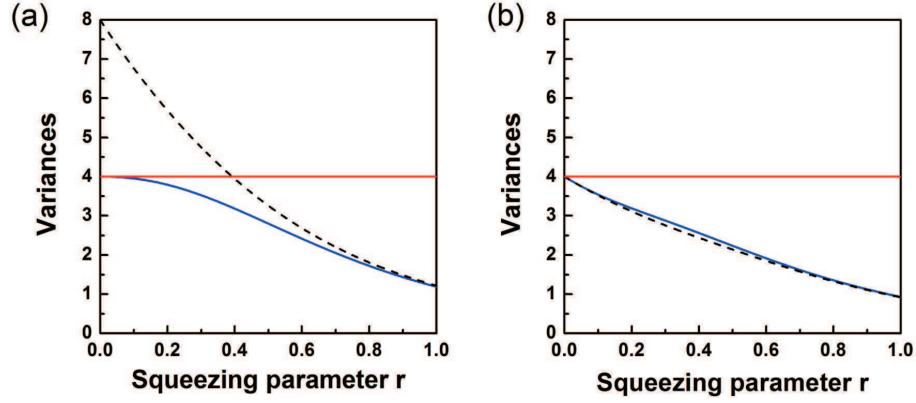


FIG. 6: **The inseparability criteria for the obtained tripartite GHZ entangled state.** (a) and (b) correspond to the first and second inequalities in Eq. (19), respectively. The dashed and solid lines correspond to the case of unit and optimal gain factor in the classical channel, respectively.

by

$$\begin{aligned}
 V_7 &= \langle \Delta^2(\hat{x}_{D_1} - \hat{x}_{D_2}) \rangle \\
 &= \frac{[(1+2G)^2 + 3 + 3(1+G)^2]V}{6} \\
 &\quad + \frac{[2(-1+G)^2 + 3(1-G)^2]V'}{6}, \\
 V_8 &= \langle \Delta^2(\hat{p}_{D_1} + \hat{p}_{D_2} + g_7\hat{p}_{D_3}) \rangle \\
 &= \frac{[2(1+G+g_7)^2 + 3(G+1)^2]V}{6} \\
 &\quad + \frac{[(2G-1-g_7)^2 + 3(1-g_7)^2 + 3(G-1)^2]V'}{6}, \\
 V_9 &= \langle \Delta^2(\hat{x}_{D_2} - \hat{x}_{D_3}) \rangle = 2V, \\
 V_{10} &= \langle \Delta^2(g_8\hat{p}_{D_1} + \hat{p}_{D_2} + \hat{p}_{D_3}) \rangle \\
 &= \frac{[2(2+Gg_8)^2 + 3(Gg_8+g_8)^2]V}{6} \\
 &\quad + \frac{[4(Gg_8-1)^2 + 3(Gg_8-g_8)^2]V'}{6}.
 \end{aligned} \tag{20}$$

When $\eta = 1$, the optimal gain in classical channel is expressed by

$$G = \frac{V' - V}{V' + V}. \tag{21}$$

The optimal gain g_j ($j = 7, 8$) to minimize the left-hand sides of the inequalities are

$$\begin{aligned}
 g_7 &= \frac{2V'(V' - V)}{(V' + V)(2V' + V)}, \\
 g_8 &= \frac{2(V' - V)^2(V' + V)}{2V'^3 + 3V'^2V + 6V'V^2 + V^3}.
 \end{aligned} \tag{22}$$

Fig. 6 shows the dependence of inseparability criteria of tripartite GHZ entangled state on squeezing parameter. The optimal gains g_j ($j = 7, 8$) in Eq. (22) are chosen in the calculation. If the unit gain is chosen, the obtained state is entangled only when the squeezing parameter is higher than 0.39 (-3.41 dB squeezing, dashed lines). When the optimal gain factor $G = 0.95$ is chosen, the requirement to the squeezing level is reduced for achieving resultant entangled state (solid lines).

D. Covariance matrix of the output state

Gaussian state is the state with Gaussian characteristic functions and quasi-probability distributions on the multi-mode quantum phase space, which can be completely characterized by a covariance matrix. The elements of the covariance matrix are $\sigma_{ij} = \text{Cov}(\hat{R}_i, \hat{R}_j) = \frac{1}{2} \langle \hat{R}_i \hat{R}_j + \hat{R}_j \hat{R}_i \rangle - \langle \hat{R}_i \rangle \langle \hat{R}_j \rangle$, where $\hat{R} = (\hat{x}_{D_1}, \hat{p}_{D_1}, \hat{x}_{D_2}, \hat{p}_{D_2}, \hat{x}_{D_3}, \hat{p}_{D_3})^T$ is a vector composed by the amplitude and phase quadratures of tripartite optical beams. Thus the covariance matrix of the tripartite optical beams is expressed as

$$\sigma = \begin{bmatrix} \sigma_{D_1} & \sigma_{D_1 D_2} & \sigma_{D_1 D_3} \\ \sigma_{D_1 D_2}^T & \sigma_{D_2} & \sigma_{D_2 D_3} \\ \sigma_{D_1 D_3}^T & \sigma_{D_2 D_3}^T & \sigma_{D_3} \end{bmatrix}, \quad (23)$$

where

$$\begin{aligned} \sigma_{D_1} &= \begin{bmatrix} \Delta^2 \hat{x}_{D_1} & 0 \\ 0 & \Delta^2 \hat{p}_{D_1} \end{bmatrix}, \\ \sigma_{D_2} &= \begin{bmatrix} \Delta^2 \hat{x}_{D_2} & 0 \\ 0 & \Delta^2 \hat{p}_{D_2} \end{bmatrix}, \\ \sigma_{D_3} &= \begin{bmatrix} \Delta^2 \hat{x}_{D_3} & 0 \\ 0 & \Delta^2 \hat{p}_{D_3} \end{bmatrix}, \\ \sigma_{D_1 D_2} &= \begin{bmatrix} \text{Cov}(\hat{x}_{D_1}, \hat{x}_{D_2}) & \text{Cov}(\hat{x}_{D_1}, \hat{p}_{D_2}) \\ \text{Cov}(\hat{p}_{D_1}, \hat{x}_{D_2}) & \text{Cov}(\hat{p}_{D_1}, \hat{p}_{D_2}) \end{bmatrix}, \\ \sigma_{D_1 D_3} &= \begin{bmatrix} \text{Cov}(\hat{x}_{D_1}, \hat{x}_{D_3}) & \text{Cov}(\hat{x}_{D_1}, \hat{p}_{D_3}) \\ \text{Cov}(\hat{p}_{D_1}, \hat{x}_{D_3}) & \text{Cov}(\hat{p}_{D_1}, \hat{p}_{D_3}) \end{bmatrix}, \\ \sigma_{D_2 D_3} &= \begin{bmatrix} \text{Cov}(\hat{x}_{D_2}, \hat{x}_{D_3}) & \text{Cov}(\hat{x}_{D_2}, \hat{p}_{D_3}) \\ \text{Cov}(\hat{p}_{D_2}, \hat{x}_{D_3}) & \text{Cov}(\hat{p}_{D_2}, \hat{p}_{D_3}) \end{bmatrix}, \end{aligned} \quad (24)$$

respectively.

For the output modes D_1 , D_2 and D_3 in a lossy channel, we have

$$\begin{aligned} \Delta^2 \hat{x}_{D_1} &= \frac{4G^2\eta + 3(1+G)^2}{6}V \\ &\quad + \frac{2G^2\eta + 3(1-G)^2}{6}V' + G^2(1-\eta), \\ \Delta^2 \hat{p}_{D_1} &= \frac{2G^2\eta + 3(1+G)^2}{6}V \\ &\quad + \frac{4G^2\eta + 3(G-1)^2}{6}V' + G^2(1-\eta), \\ \Delta^2 \hat{x}_{D_2} &= \Delta^2 \hat{x}_{D_3} = \frac{2}{3}V + \frac{1}{3}V', \\ \Delta^2 \hat{p}_{D_2} &= \Delta^2 \hat{p}_{D_3} = \frac{1}{3}V + \frac{2}{3}V', \\ \text{Cov}(\hat{x}_{D_1}, \hat{x}_{D_2}) &= \text{Cov}(\hat{x}_{D_1}, \hat{x}_{D_3}) = -\frac{G\sqrt{\eta}}{3}V + \frac{G\sqrt{\eta}}{3}V', \\ \text{Cov}(\hat{p}_{D_1}, \hat{p}_{D_2}) &= \text{Cov}(\hat{p}_{D_1}, \hat{p}_{D_3}) = -\frac{G\sqrt{\eta}}{3}V' + \frac{G\sqrt{\eta}}{3}V, \end{aligned} \quad (25)$$

$$\begin{aligned} \text{Cov}(\hat{x}_{D_2}, \hat{x}_{D_3}) &= -\frac{1}{3}V + \frac{1}{3}V', \\ \text{Cov}(\hat{p}_{D_2}, \hat{p}_{D_3}) &= -\frac{1}{3}V' + \frac{1}{3}V, \\ \text{Cov}(\hat{x}_{D_1}, \hat{p}_{D_2}) &= \text{Cov}(\hat{p}_{D_1}, \hat{x}_{D_2}) = 0, \\ \text{Cov}(\hat{x}_{D_1}, \hat{p}_{D_3}) &= \text{Cov}(\hat{p}_{D_1}, \hat{x}_{D_3}) = 0, \\ \text{Cov}(\hat{x}_{D_2}, \hat{p}_{D_3}) &= \text{Cov}(\hat{p}_{D_2}, \hat{x}_{D_3}) = 0. \end{aligned}$$

To partially reconstruct all relevant entries of its associated covariance matrix, we have performed 18 different measurements on the output optical modes. These measurements include the variances of the amplitude and phase quadratures of three output optical modes, and the cross correlation variances $\Delta^2(\hat{x}_{D_1} - \hat{x}_{D_2})$, $\Delta^2(\hat{x}_{D_1} - \hat{x}_{D_3})$, $\Delta^2(\hat{x}_{D_2} - \hat{x}_{D_3})$, $\Delta^2(\hat{p}_{D_1} + \hat{p}_{D_2})$, $\Delta^2(\hat{p}_{D_1} + \hat{p}_{D_3})$, $\Delta^2(\hat{p}_{D_2} + \hat{p}_{D_3})$, $\Delta^2(\hat{x}_{D_1} + \hat{p}_{D_2})$, $\Delta^2(\hat{x}_{D_2} + \hat{p}_{D_1})$, $\Delta^2(\hat{x}_{D_1} + \hat{p}_{D_3})$, $\Delta^2(\hat{x}_{D_3} + \hat{p}_{D_1})$, $\Delta^2(\hat{x}_{D_2} + \hat{p}_{D_3})$ and $\Delta^2(\hat{x}_{D_3} + \hat{p}_{D_2})$, respectively. The covariance elements are calculated via [41]

$$\begin{aligned} \text{Cov}(\hat{R}_i, \hat{R}_j) &= \frac{1}{2} \left[\Delta^2(\hat{R}_i + \hat{R}_j) - \Delta^2 \hat{R}_i - \Delta^2 \hat{R}_j \right], \\ \text{Cov}(\hat{R}_i, \hat{R}_j) &= -\frac{1}{2} \left[\Delta^2(\hat{R}_i - \hat{R}_j) - \Delta^2 \hat{R}_i - \Delta^2 \hat{R}_j \right]. \end{aligned} \quad (26)$$

In the experiment, we obtain all the covariance matrices of every quantum state actually, and then calculate the PPT eigenvalues to verify whether the quantum states are entangled or not.

In our experiment, the squeezing and anti-squeezing noises of squeezed states are -5.90 dB and 9.84 dB, which correspond to $V = 0.26$ and $V' = 9.64$, respectively. The optimal gain $G = 0.85$ is chosen to optimize PPT eigenvalues. We measured covariance matrix of the output modes D_1 , D_2 and D_3 with different transmission efficiency $\eta = 0.98, 0.80, 0.60, 0.40$ and 0.20 , the reconstructed covariance matrix are

$$\sigma_1 = \begin{pmatrix} 3.05 & 0 & 2.74 & 0.21 & 2.67 & 0.07 \\ 0 & 5.34 & -0.20 & -2.54 & -0.15 & -2.88 \\ 2.74 & -0.20 & 3.46 & 0 & 3.13 & 0.01 \\ 0.21 & -2.54 & 0 & 6.37 & 0.25 & -2.94 \\ 2.67 & -0.15 & 3.13 & 0.25 & 3.36 & 0 \\ 0.07 & -2.88 & 0.01 & -2.94 & 0 & 6.68 \end{pmatrix}, \quad (27)$$

$$\sigma_2 = \begin{pmatrix} 2.68 & 0 & 2.44 & 0.11 & 2.50 & 0.11 \\ 0 & 4.75 & -0.08 & -2.42 & -0.18 & -2.51 \\ 2.44 & -0.08 & 3.51 & 0 & 3.31 & 0.13 \\ 0.11 & -2.42 & 0 & 6.44 & 0.02 & -3.08 \\ 2.50 & -0.18 & 3.31 & 0.02 & 3.67 & 0 \\ 0.11 & -2.51 & 0.13 & -3.08 & 0 & 6.53 \end{pmatrix}, \quad (28)$$

$$\sigma_3 = \begin{pmatrix} 2.39 & 0 & 2.17 & 0.15 & 2.24 & -0.03 \\ 0 & 3.89 & 0.008 & -1.97 & -0.13 & -2.24 \\ 2.17 & 0.008 & 3.51 & 0 & 3.31 & 0.06 \\ 0.15 & -1.97 & 0 & 6.44 & 0.02 & -3.16 \\ 2.24 & -0.13 & 3.31 & 0.02 & 3.67 & 0 \\ -0.03 & -2.24 & 0.06 & -3.16 & 0 & 6.68 \end{pmatrix}, \quad (29)$$

$$\sigma_4 = \begin{pmatrix} 1.92 & 0 & 1.72 & 0.42 & 1.80 & 0.30 \\ 0 & 2.93 & -0.03 & -1.57 & -0.07 & -1.60 \\ 1.72 & -0.03 & 3.51 & 0 & 3.31 & 0.06 \\ 0.42 & -1.57 & 0 & 6.44 & 0.02 & -3.16 \\ 1.80 & -0.07 & 3.31 & 0.02 & 3.67 & 0 \\ 0.30 & -1.60 & 0.06 & -3.16 & 0 & 6.68 \end{pmatrix}, \quad (30)$$

$$\sigma_5 = \begin{pmatrix} 1.56 & 0 & 1.20 & 0.27 & 1.29 & 0.28 \\ 0 & 2.23 & -0.16 & -1.16 & -0.18 & -1.17 \\ 1.20 & -0.16 & 3.51 & 0 & 3.31 & 0.13 \\ 0.27 & -1.16 & 0 & 6.44 & 0.02 & -3.08 \\ 1.29 & -0.18 & 3.31 & 0.02 & 3.67 & 0 \\ 0.28 & -1.17 & 0.13 & -3.08 & 0 & 6.53 \end{pmatrix}, \quad (31)$$

respectively. The entanglement among the prepared tripartite state is evaluated by PPT criterion and we obtain PPT eigenvalues $\text{PPT}_{D_1} = 0.52$, $\text{PPT}_{D_2} = 0.39$, $\text{PPT}_{D_3} = 0.40$ for $\eta = 0.98$, and $\text{PPT}_{D_1} = 0.61$, $\text{PPT}_{D_2} = 0.42$, $\text{PPT}_{D_3} = 0.42$ for $\eta = 0.80$, and $\text{PPT}_{D_1} = 0.74$, $\text{PPT}_{D_2} = 0.50$, $\text{PPT}_{D_3} = 0.50$ for $\eta = 0.60$, and $\text{PPT}_{D_1} = 0.86$, $\text{PPT}_{D_2} = 0.58$, $\text{PPT}_{D_3} = 0.56$ for $\eta = 0.40$, and $\text{PPT}_{D_1} = 1.03$, $\text{PPT}_{D_2} = 0.70$, $\text{PPT}_{D_3} = 0.66$ for $\eta = 0.20$, respectively.

-
- [1] H. J. Briegel and R. Raussendorf, Phys. Rev. Lett. **86**, 910 (2001).
[2] J. Zhang and S. L. Braunstein, Phys. Rev. A **73**, 032318 (2006).
[3] R. Raussendorf and H. J. Briegel, Phys. Rev. Lett. **86**, 5188 (2001).
[4] N. C. Menicucci, P. van Loock, M. Gu, C. Weedbrook, T. C. Ralph, and M. A. Nielsen, Phys. Rev. Lett. **97**, 110501 (2006).
[5] R. Ukai, N. Iwata, Y. Shimokawa, S. C. Armstrong, A. Politi, J. I. Yoshikawa, P. van Loock, and A. Furusawa, Phys. Rev. Lett. **106**, 240504 (2011).
[6] X. Su, S. Hao, X. Deng, L. Ma, M. Wang, X. Jia, C. Xie, and K. Peng, Nat. Commun. **4**, 2828 (2013).
[7] P. van Loock and S. L. Braunstein, Phys. Rev. Lett. **84**, 3482 (2000).
[8] H. Yonezawa, T. Aoki, and A. Furusawa, Nature (London) **431**, 430 (2004).
[9] J. Jing, J. Zhang, Y. Yan, F. Zhao, C. Xie, and K. Peng, Phys. Rev. Lett. **90**, 167903 (2003).
[10] J. Roslund, R. M. de Araújo, S. Jiang, C. Fabre, and N. Treps, Nat. Photonics **8**, 109 (2014).
[11] D. E. Browne and T. Rudolph, Phys. Rev. Lett. **95**, 010501 (2005).
[12] Y. Miwa, R. Ukai, J.-I. Yoshikawa, R. Filip, P. van Loock, and A. Furusawa, Phys. Rev. A **82**, 032305 (2010).
[13] S. Bose, V. Vedral, and P. L. Knight, Phys. Rev. A **57**, 822 (1998).
[14] P. Kómár, E. M. Kessler, M. Bishof, L. Jiang, A. S. Sørensen, J. Ye, and M. D. Lukin, Nat. Phys. **10**, 582 (2014).
[15] J. Yin *et al.* Nature (London) **488**, 185 (2012).
[16] X.-S. Ma *et al.* Nature (London) **489**, 269 (2012).
[17] H. Takesue, S. D. Dyer, M. J. Stevens, V. Verma, R. P. Mirin, and S.W. Nam, Optica **2**, 832 (2015).
[18] M. Żukowski, A. Zeilinger, M. A. Horne, and A. K. Ekert, Phys. Rev. Lett. **71**, 4287 (1993).
[19] J.-W. Pan, D. Bouwmeester, H. Weinfurter, and A. Zeilinger, Phys. Rev. Lett. **80**, 3891 (1998).
[20] F. Sciarrino, E. Lombardi, G. Milani, and F. De Martini, Phys. Rev. A **66**, 024309 (2002).
[21] H. de Riedmatten, I. Marcikic, J. A. W. van Houwelingen, W. Tittel, H. Zbinden, and N. Gisin, Phys. Rev. A **71**, 050302(R) (2005).
[22] R. E. S. Polkinghorne and T. C. Ralph, Phys. Rev. Lett. **83**, 2095 (1999).
[23] S. M. Tan, Phys. Rev. A **60**, 2752 (1999).
[24] P. van Loock and S. L. Braunstein, Phys. Rev. A **61**, 010302(R) (1999).
[25] X. Jia, X. Su, Q. Pan, J. Gao, C. Xie, and K. Peng, Phys. Rev. Lett. **93**, 250503 (2004).
[26] N. Takei, H. Yonezawa, T. Aoki, and A. Furusawa, Phys. Rev. Lett. **94**, 220502 (2005).
[27] S. Takeda, M. Fuwa, P. van Loock, and A. Furusawa, Phys. Rev. Lett. **114**, 100501 (2015).
[28] U. L. Andersen, J. S. Neergaard-Nielsen, P. van Loock, and A. Furusawa, Nat. Phys. **11**, 713 (2015).
[29] C.-Y. Lu, T. Yang, and J.-W. Pan, Phys. Rev. Lett. **103**, 020501 (2009).
[30] Y. Zhou, X. Jia, F. Li, C. Xie, and K. Peng, Opt. Express, **23**, 4952 (2015).
[31] X. Su, A. Tan, X. Jia, J. Zhang, C. Xie, and K. Peng, Phys. Rev. Lett. **98**, 070502 (2007).
[32] P. van Loock and A. Furusawa, Phys. Rev. A **67**, 052315 (2003).
[33] R. F. Werner and M. M. Wolf, Phys. Rev. Lett. **86**, 3658 (2001).
[34] G. Adesso, A. Serafini, and F. Illuminati, Phys. Rev. A **73**, 032345 (2006).
[35] C. E. Vollmer, D. Schulze, T. Eberle, V. Händchen, J.

- Fiurášek, and R. Schnabel, Phys. Rev. Lett. **111**, 230505 (2013).
- [36] H. Vahlbruch, M. Mehmet, K. Danzmann, and R. Schnabel. Phys. Rev. Lett. **117**, 110801 (2016).
- [37] T. C. Ralph, Phys. Rev. A **84**, 022339 (2011).
- [38] H. M. Chrzanowski, N. Walk, S. M. Assad, J. Janousek, S. Hosseini, T. C. Ralph, T. Symul, and P. K. Lam, Nat. Photonics **8**, 333 (2014).
- [39] A. E. Ulanov, I. A. Fedorov, A. A. Pushkina, Y. V. Kurochkin, T. C. Ralph, and A. I. Lvovsky, Nat. Photonics **9**, 764 (2015).
- [40] M. Lassen, A. Berni, L. S. Madsen, R. Filip, and U. L. Andersen, Phys. Rev. Lett. **111**, 180502 (2013).
- [41] S. Steinlechner, J. Bauchrowitz, T. Eberle, and R. Schnabel, Phys. Rev. A **87**, 022104 (2013).